On the Origin of Kinesin Limping

Adrian N. Fehr,[†] Braulio Gutiérrez-Medina,[‡] Charles L. Asbury,[§] and Steven M. Block[†‡*]
[†]Departments of Applied Physics and [‡]Biology, Stanford University, Stanford, California, and [§]Department of Physiology and Biophysics, University of Washington, Seattle, Washington

ABSTRACT   Kinesin is a dimeric motor with twin catalytic heads joined to a common stalk. Kinesin molecules move processively along microtubules in a hand-over-hand walk, with the two heads advancing alternately. Recombinant kinesin constructs with short stalks have been found to "limp", i.e., exhibit alternation in the dwell times of successive steps. Limping behavior implies that the molecular rearrangements underlying even- and odd-numbered steps must differ, but the mechanism by which such rearrangements lead to limping remains unsolved. Here, we used an optical force clamp to measure individual, recombinant dimers and test candidate explanations for limping. Introducing a covalent cross-link into the stalk region near the heads had no effect on limping, ruling out possible stalk misregistration during coiled-coil formation as a cause. Limping was equally unaffected by mutations that produced 50-fold changes in stalk stiffness, ruling out models where limping arises from an asymmetry in torsional strain. However, limping was enhanced by perturbations that increased the vertical component of load on the motor, including increases in bead size or net load, and decreases in the stalk length. These results suggest that kinesin heads take different vertical trajectories during alternate steps, and that the rates for these motions are differentially sensitive to load.

INTRODUCTION

Conventional kinesin motors (kinesin-1) carry two identical catalytic domains (heads) that each hydrolyze ATP and can bind to a microtubule (MT). The heads are attached via neck linkers to a common stalk, which consists mainly of a lengthy (~70 nm) α-helical, coiled-coil region with occasional structural interruptions ("hinges"). The neck linkers join at a dimerization domain proximal to the heads, the ~35-residue neck coiled coil (Fig. 1 A). The individual kinesin heads carry out a hand-over-hand walk that moves the molecule toward the plus-end of a MT stepwise, in 8-nm increments (1–3), generated as each motor domain executes a 16-nm motion past its partner that is tightly coupled to the hydrolysis of a single ATP molecule (4–6). A hallmark of kinesin motility is its processivity, the ability to take hundreds of steps before releasing the MT, even against pN-scale loads (7–10).

Certain kinesin molecules exhibit "limping", i.e., alternating short- and long-average dwell intervals between steps. Limping was anticipated for heterodimeric constructs carrying one wild-type and one mutant motor domain with a diminished capacity to hydrolyze ATP (2). However, limping was also found in certain homodimeric constructs, composed of otherwise identical polypeptide chains. Here, the underlying cause is more subtle and has remained the subject of inquiry. Regardless of the cause, the existence of limping in kinesin implies that it moves by an "asymmetric, hand-over-hand" walk, where the even- and odd-numbered steps are nonidentical (1,11). Measurements with homodimeric constructs of various stalk lengths showed that the severity of limping for a given, fixed load increases as the

number of amino acids in the stalk is reduced (1). Furthermore, the limping of short-stalk constructs was more severe at increased longitudinal load ((11); see below). These data are consistent with (at least) three possible models to explain the cause of limping: misregistration, winding, and vertical loading (1,12).

In the misregistration model, the α-helices of the coiled-coil stalk are proposed to shift axially relative to one another, possibly due to coiled-coil breathing (13). The effect of this misregistration is to produce a small difference in the lengths of the neck linkers. A misalignment by just one heptad repeat would introduce an increase of ~1 nm in the tether between the one head and the stalk, placing the associated motor domain farther from the next MT binding site and slowing its kinetics relative to its unshifted partner. The model accounts for the increased tendency of short constructs to limp because abbreviated coiled coils are less stable energetically and therefore more prone to misregistration. In the winding model, limping is proposed to result from an anisotropy in the torsional stiffness of the stalk (1,7,11,14). Hand-over-hand motion during an asymmetric walk generates twist in the stalk, winding it in alternate rotational senses at each step. If the energetic barrier to twist one direction differs from the other, then this asymmetry could differentially affect the kinetics of alternate steps. Moreover, any such energetic asymmetry would be expected to decrease for longer constructs, which are torsionally more compliant. Sensitivity to torsional stiffness could arise in various ways. For example, coiled coils have left-handed chirality, so the torsional stiffness for overwinding may differ from that of underwinding (15). The last of the three candidate explanations, vertical loading, is motivated by work showing that forces directed perpendicular to the MT long axis can affect stepping kinetics (16,17). Sensitivity to vertical loads
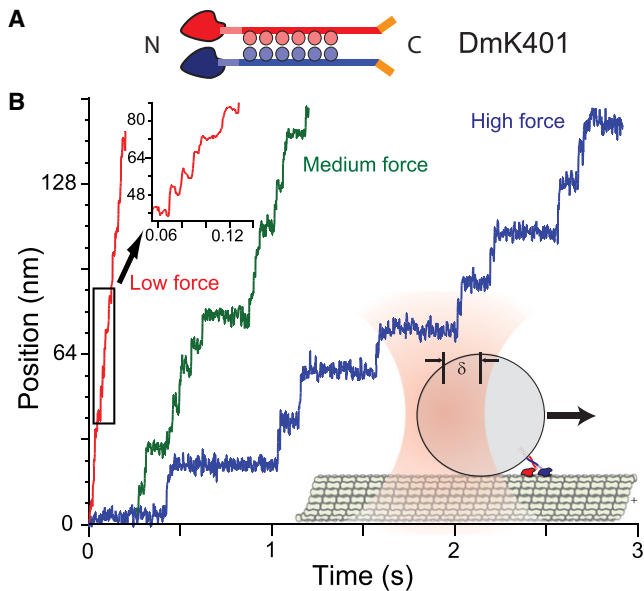
FIGURE 1   Kinesin structure and stepping records. (*A*) Cartoon representation of DmK401, oriented with N- and C-termini as shown. Each molecule is composed of two heavy chains (*light* and *dark gray*, *red* and *blue* online) with N-terminal motor domains (*dark shaded regions*) joined by neck linkers (*light shaded lines*) to the coiled coil stalk (*straight lines*), containing heptad motif repeats (*circles*) that associate to form a coiled coil. The heavy chains of constructs were truncated and terminated by 6×-His tags (*bent short lines*) to bind anti-His antibody-coated beads. (*B*) Representative stepping records of single molecules of DmK401 versus time, recorded under force-clamped conditions with an optical trap (*light gray, red* online, −2.5 pN; *medium gray, green* online, −3.7 pN; *dark gray, blue* online, −4.7 pN). The stepwise advances and intervals during which the kinesin molecule dwells can be clearly visualized: note that as load increases, the step intervals increasingly alternate between short and long times, i.e., the molecule "limps". (*Left inset*) Expanded view of the *light gray* (*red* online) trace, showing steps resolved despite the higher speed. (*Right inset*) Cartoon of the kinesin bead assay (not to scale), showing the optical trap (*fading gray, pink* online) acting on a small bead (*gray*). The kinesin molecule (*dark gray, red* and *blue* online) moves on the MT (*light gray structure, green* online) and pulls the bead in the direction shown. Feedback is used to maintain the trap at a fixed distance behind the bead, which results in the kinesin motor experiencing constant force.

was interpreted as evidence that some portion of the molecule important for mechanochemistry, e.g., the neck linkers, or the N-terminus of the neck coiled coil, may rise and fall relative to the MT surface during each kinetic cycle. Indeed, this idea has been incorporated into theoretical models for stepping, for non-limping motors (18), and for the specific case of limping where the two heads rise and fall by differing amounts (12).

To test all three candidate explanations, we used a high-resolution optical trap equipped with a force clamp (19,20) to measure the limping properties of recombinant kinesin-1 constructs based on the *Drosophila* gene. Parallel to work with human kinesin (13), we created constructs with coiled coils that could be reversibly cross-linked to probe directly the intramolecular register of the α-helices. To measure the torsional properties of recombinant molecules bound to

MTs, we used a new fluorescence-based assay to follow the thermally driven motions of beads attached to the stalk (B. Gutiérrez-Medina, Adrian N. Fehr, and Steven M. Block, unpublished), characterizing constructs with a ~50-fold range of stiffness. These data were then correlated with the severity of limping obtained from force-clamped records of movement. Finally, we modulated the degree of vertical loading on single molecules by carrying out force-clamped assays using a variety of bead sizes over a range of retarding loads.

MATERIALS AND METHODS

Protein preparation

Expression plasmids for DmK401 (pCA1) and DmK448 (pAF1) were previously described (1). To make a cysteine-light version of DmK401 (pAF13), the locations of solvent-exposed cysteines (C45 and C338) were identified by homology mapping the DmK peptide sequence against the human kinesin motor domain crystal structure (Protein Data Bank file 1BG2) and the appropriate residues were changed to serine by site-directed mutagenesis. The removal of reactive cysteines was verified by incubating purified protein with the oxidizer 5, 5′-dithiobis-(2-nitrobenzoate) (DTNB; 0.2 mM), for 60 min at room temperature and comparing any cross-linking present against samples reduced by dithiothreitol (DTT; 2 mM), assayed by SDS-PAGE gel (13). Image processing of the gel (ImageJ; http://rsb.info.nih.gov/ij/) was used to quantify the relative intensity of monomers and dimers. Further site-directed mutagenesis was carried out on pAF13 to introduce cysteines into the neck coiled-coil region, to produce the expression plasmids Y352C (pAF14) and N359C (pAF15).

DmK401-StableCoil, a mutant similar to DmK401 (which is terminated by a four-residue linker followed by a 6×-histidine tag), was engineered with the non-coiled-coil-forming residues near the C-terminus of the stalk (as predicted by COILS (21)) replaced by cassette mutagenesis with four consecutive, in-register stable coil repeats, (i.e., 378 DmK residues followed by 28 stable coil residues and a 6×-histidine tag). The C-terminal peptide sequence for plasmid pAF21 is therefore R_{375}WRA*EIEALKAEIEALKAEIEALKAEI EALKA*HHHHHH (stable coil residues italicized). All mutations were verified by sequencing.

BL21(DE3) *Escherichia coli* were transformed with expression plasmids as previously described (1). All constructs were subsequently purified to homogeneity by affinity-based fast protein liquid chromatography. Clarified lysates were mixed 1:4 with binding buffer (50 mM NaPO₄, 60 mM imidazole, 250 mM NaCl, 1 mM MgCl₂, 2 mM DTT, 10 μM ATP, pH 8.0) and incubated on histidine-binding columns (HisTrap FF Crude; GE Healthcare, Piscataway, NJ) at 4°C for 8 h. Columns were washed (buffer same as binding buffer, but at pH 6.0) and kinesin protein was eluted by an imidazole gradient (buffer same as binding buffer, but with 0.5 M imidazole, pH 7.0). Kinesin fractions were pure, judged by SDS-PAGE, and stored in 50% glycerol at −20°C until use.

In vitro motility assays

Biotinylated penta-His antibody (Qiagen, Valencia, CA) was incubated with streptavidin-coated polystyrene beads (Spherotech, Lake Forest, IL) and mixed with dilute kinesin protein in assay buffer (80 mM Pipes, 50 mM KAc, 4 mM MgCl₂, 2 mM DTT, 1 mM EGTA, 7 μM taxol, 2 mg/ml BSA, pH 6.9). All experiments were carried out in 2 mM ATP, except when ATP dependence was assayed. Before use, an oxygen scavenging system was added to the kinesin mixture: 235 μg/ml glucose oxidase, 42 μg/ml catalase, and 4.6 mg/ml glucose. Motility assays under oxidizing conditions were carried out with assay buffer as described, except that 0.2 mM DTNB was used in place of DTT. Other reagents in the assay buffer did not affect the kinesin cross-linking efficiency, as measured by SDS-PAGE.

The optical trap was used to place kinesin-coated beads near taxol-stabilized MTs that had been immobilized on a cover glasses by polylysine (1,6,19,22). Bead position was monitored by a separate detection laser focused to a diffraction-limited spot and relayed onto a position-sensitive detector (23,24). Data were acquired at 20 kHz, decimated to 2 kHz, and filtered at the Nyquist frequency of 1 kHz. During kinesin stepping, the trap position was steered by acousto-optic deflectors to maintain a fixed distance between the bead and trap center using computer-based feedback (200 Hz update rate), supplying constant (longitudinal) force (19,20,22). Records were only collected from kinesin assays sufficiently dilute so that fewer than half the tested beads moved, to ensure measurements in the single-molecule regime (8).

The position response of the steering and detection optics was calibrated using a three-axis piezoelectric stage (Physik Instrumente, Karlsruhe, Germany) and a National Institute of Standards and Technology-traceable objective micrometer. Stiffness of the optical trap was calibrated by three methods: using the Equipartition theorem, the thermal power spectrum, and viscous drag force on a bead produced by moving the stage (reviewed in Neuman and Block (25)). The power-spectrum and Equipartition methods are based on thermally driven motions, and therefore only probe the central ~30 nm of the trap (for stiffnesses around ~0.05 pN/nm), whereas viscous drag can be used to map the trap stiffness profile well beyond its center. Within the linear (Hookean) region of our trap (± 100 nm from center), all three methods were in good agreement (within 20%). At larger distances, the stiffness becomes sublinear with position, as measured by the viscous drag method. Here, we operated the force clamp with a bead-trap separation of 80–100 nm.

Torsion assays

Streptavidin-coated beads, 1.27-μm in diameter (Spherotech, Lake Forest, IL), were incubated in phosphate buffer with stoichiometric amounts of 200-nm diameter fluorescent, biotinylated beads (Molecular Probes, Eugene, OR), which served as markers (see Results). This incubation results in an admixture of large beads with 0, 1, 2, or more markers beads bound. An excess of biotinylated anti-histidine antibody (Qiagen) was incubated with the bead complexes followed by washes to remove unbound antibody. Complexes were resuspended in assay buffer (with 2 μM AMP-PNP replacing ATP), diluted to picomolar concentration, and mixed with serially diluted kinesin constructs, such that roughly half the beads had bound motors, as judged by MT binding. For measurements, the AMP-PNP concentration was increased to 2 mM and bead complexes were introduced into flow cells containing surface-immobilized MTs, as previously described. Complexes with diametrically opposed fluorescent beads were selected under epifluorescence, then the microscope imaging mode was switched to Nomarski differential interference contrast and used to position the selected complexes near MTs. In addition to stabilizing kinesin-MT binding with 2 mM AMP-PNP (10), DmK448 constructs were also cross-linked directly to MTs using 2 mM 1-ethyl-3-[3-dimethylaminopropyl]carbodiimide (EDC) and 5 mM N-hydroxysuccinimide (Sulfo-NHS). To avoid unwanted bonds, chemical cross-linking was performed stepwise, by first incubating MTs with EDC and Sulfo-NHS for 12 min, followed by washes using 10-kDa centrifuge filters (PALL, Port Washington, NY), and finally incubating activated MTs with kinesin in the presence of 2 mM AMP-PNP for 40 min. During fluorescence data collection, the trapping laser and bright-field illumination were shuttered; images were acquired at 28 Hz by a cooled charge-coupled device camera (Cascade; Princeton Instruments, Trenton, NJ).

The (x, y) coordinates of the fluorescent marker beads were obtained by centroid tracking, using software written in LabView 7.0 (National Instruments, Austin, TX). Joining the centroid positions by a line, we computed the angle relative to the camera reference frame. From each record of angle versus time, the variance was calculated as a function of the lag time, τ, between data points in the file. The torsional stiffness was computed by fitting the variance data, $\langle \xi^2(\tau) \rangle$, to $\langle \xi^2(\tau) \rangle = (k_B T / \kappa_\xi)(1 - \exp[-\tau/\tau_o])$.

Data analysis

Stepping data were analyzed with software written in Igor Pro 5.0 (Wave-Metrics, Lake Oswego, OR) as previously described (1,26). Computations of the effective angle of applied load were based on the following assumptions (1): i), the kinesin length, l_o, is dominated by the coiled coil of the stalk, which is assumed to have a rise of 0.15 nm per amino acid residue (27); ii), the antibody-based linkage between kinesin and the bead adds an effective length, l_α, to each construct of 10 nm (except for native squid kinesin, where the attachment was nonspecific); and iii), beads tend to be held by the optical trap directly against the MT surface.

RESULTS

The motions of individual kinesin molecules bound to beads and moving on MTs were recorded under force-clamped conditions with nm-scale resolution at kHz bandwidths (Fig. 1 B) (19,20). We identified all the stepping dwells in a given single-molecule record ("run"), as previously described (1,26), creating even- and odd-numbered sets of steps. We then calculated the average duration for each set. The set with the longer average was assigned to the "slow phase" and the set with the shorter average was assigned to the "fast phase". The ratio of the average times for the slow phase to the fast phase in each run was taken as a dimensionless measure of limping, the limp factor, L. Limp factors from multiple runs for an ensemble of different molecules were then averaged under each set of assay conditions to provide a global measure of limping.

To test the misregistration model, we engineered a construct with a pair of apposed cysteine residues in the neck coiled-coil region that could be cross-linked. Data from this mutant can be used to reveal whether misregistration occurs, and, when such shifts are prevented, whether molecules continue to limp. The cysteines were joined with high efficiency by a disulfide bond under oxidizing conditions (with the addition of DTNB to the buffer) that could be reversibly reduced (with DTT). Briefly, we created a "Cys-light" variant of DmK401 by replacing all solvent-exposed cysteines with serine, then replaced Asp-359, which is buried in the hydrophobic core of the neck coiled coil, with cysteine (N359C) (Fig. 2 A). To confirm that Cys-light DmK401 had no reactive cysteines, we incubated the motor with 0.2 mM DTNB for 60 min at room temperature before running it alongside a DTT-reduced sample on a 10% acrylamide SDS-PAGE gel. We found no high molecular weight bands, indicating that any solvent-exposed cysteines were removed (Fig. 2 B). The mutations carried by the Cys-light construct did not alter its velocity or limp factor compared to the parent, DmK401 (Fig. 2 C). We then carried out the same procedure for N359C. In this case, the protein migrated to the position expected for a dimer with nearly 100% efficiency, indicating that all heavy chains had been cross-linked. This high efficiency suggests that either the neck coiled coil of N359C is never misregistered, or that over the timescale of the incubation, a sufficiently large range of axial positions is explored that the dimer can be locked into proper registration once the correct configuration is transiently
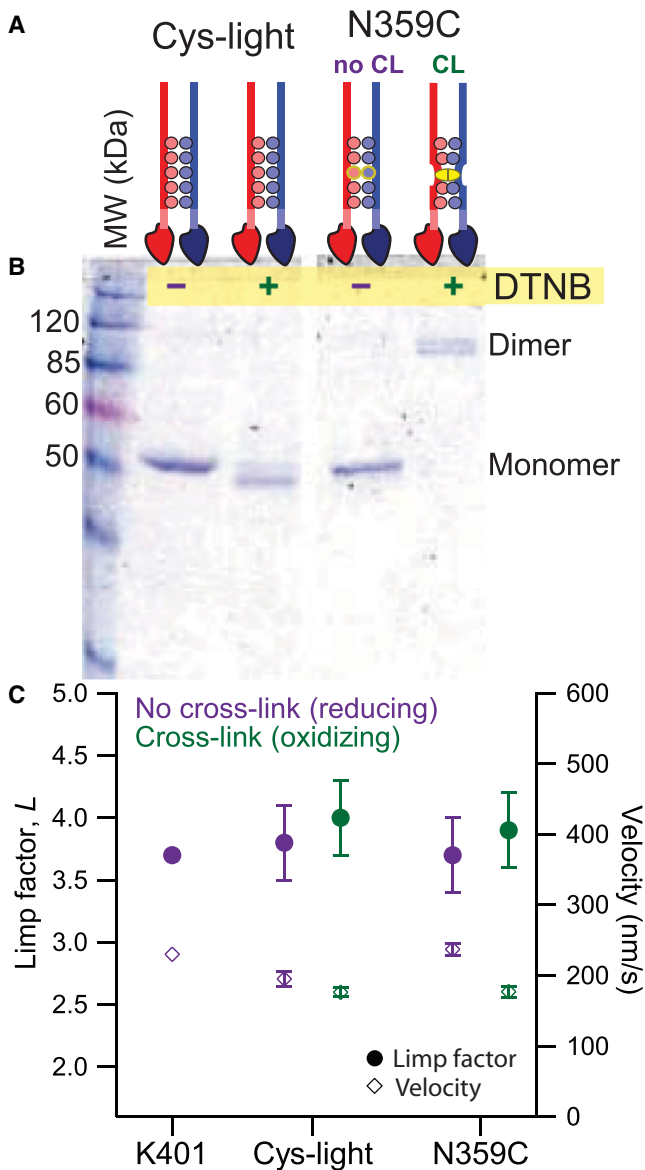
FIGURE 2 Stalk cross-linking and kinesin limping. (*A*) Cartoons of DmK Cys-light and N359C under reducing and oxidizing conditions (*gray shading*, coloring online same as in Fig. 1). Under oxidizing conditions (+DTNB), C359 residues (*faint gray, gold* online) form a disulfide bond, linking the heavy chains together in register. (*B*) Denaturing gel (SDS-PAGE) showing migration of polypeptides. Cys-light migrates as a monomer under reducing or oxidizing conditions (85% ± 5% and 98% ± 10%, respectively, of lane density corresponds to monomer), confirming that surface-reactive cysteines were removed. Under reducing conditions, N359C migrates as a monomer (93% ± 7%), but as a dimer under oxidizing conditions (108% ± 17%). (*C*) Limp factor and velocity statistics for DmK401, Cys-light and N359C. DmK401: $L = 3.7$, $v = 230$ nm/s. DmK401 values were interpolated from the data of Fig. 2 *B*. Cys-light: $L = 3.8 ± 0.3$, $v = 195 ± 10$ nm/s (reducing); $L = 4.0 ± 0.3$, $v = 176 ± 6$ nm/s (oxidizing). N359C: $L = 3.7 ± 0.3$, $v = 237 ± 9$ nm/s (reducing); $L = 3.9 ± 0.3$, $v = 177 ± 8$ nm/s (oxidizing). Each point represents data from at least 80 stepping records from 8 molecules. $F_x = -3.5$ pN.

attained. To distinguish these possibilities, we measured the motion of N359C after DTNB treatment and found that both its velocity and limp factor were statistically indistinguishable

from DmK401 and Cys-light DmK401 (Fig. 2 *C*). The finding that molecules with cross-linked, properly registered coiled coils continue to limp, and with identical kinetics to those of unlinked motors, indicates that misregistration of the coiled coil cannot be responsible for kinesin limping.

The winding model attributes limping to anisotropy in the torsional compliance, and therefore predicts that limping should correlate with the torsional stiffness of the stalk. To search for such an effect, we developed an assay to measure the stiffness of various kinesin constructs. Briefly, 1.27-μm diameter beads were sparsely labeled with smaller, 200-nm diameter fluorescent "marker" beads and then incubated with dilute kinesin. Kinesin-coated beads were positioned near surface-immobilized MTs using the optical trap and allowed to attach in the presence of 2 mM AMP-PNP, which is known to induce tight binding of the motor (10) (Fig. 3 *A*). The trapping laser was then turned off, and fluorescence imaging was used to identify those beads carrying two more-or-less diametrically opposed fluorescent markers, which were then video recorded. The positions of the two markers, driven by angular thermal motion of the central bead, were obtained by centroid tracking (Fig. 3 *B*) and transformed into records of angle versus time. From such records, the variance was computed as a function of lag time, allowing us to combine the statistics from records of multiple molecules.

We tested DmK401, a construct with a short stalk that exhibits pronounced limping, together with two constructs of similar length but different torsional properties. Compared to DmK401, DmK448 has 47 additional residues in its stalk, including a complete sequence of the so-called "hinge 1" domain, which is not predicted to form a coiled coil, and is therefore expected to decrease stalk stiffness. DmK401-StableCoil (hereafter "StableCoil"), has the C-terminal portion of hinge 1 in DmK401 replaced by four tandem repeats of a coil-forming motif, creating a single, continuous coiled coil in the stalk, which is predicted to increase torsional stiffness. Constructs with low torsional stiffness require lengthy observation times (hundreds of seconds) in our assay, so DmK448 molecules were chemically cross-linked to MTs to prevent head detachment events (see Materials and Methods). Representative records of angle for DmK401, DmK448, and StableCoil are shown in Fig. 3 *C*, and population variances for these molecules are shown in Fig. 3 *D*. Because, at equilibrium, the angular variance obeys the relation $\langle \xi^2 \rangle = k_B T / \kappa$, where $k_B T$ is the thermal energy and κ is the torsional stiffness of the bead tether, fits to variance data can be used to extract the torsional stiffnesses for these molecules: $\kappa_{DmK401} = 6.4 ± 0.4$ pN nm rad^{-1}, $\kappa_{DmK448} = 0.23 ± 0.01$ pN nm rad^{-1}, and $\kappa_{StableCoil} = 13 ± 0.4$ pN nm rad^{-1}. Despite a 26-fold decrease in stiffness, however, the limp factors for DmK401 and DmK448 were previously found to be the same within experimental error (1). Here, despite a more than twofold increase in torsional stiffness, the limp factor for StableCoil ($L_{StableCoil} = 4.5 ± 0.6$) was statistically identical to the value for DmK401 ($L_{DmK401} = 4.6 ± 0.5$), measured under a hindering load
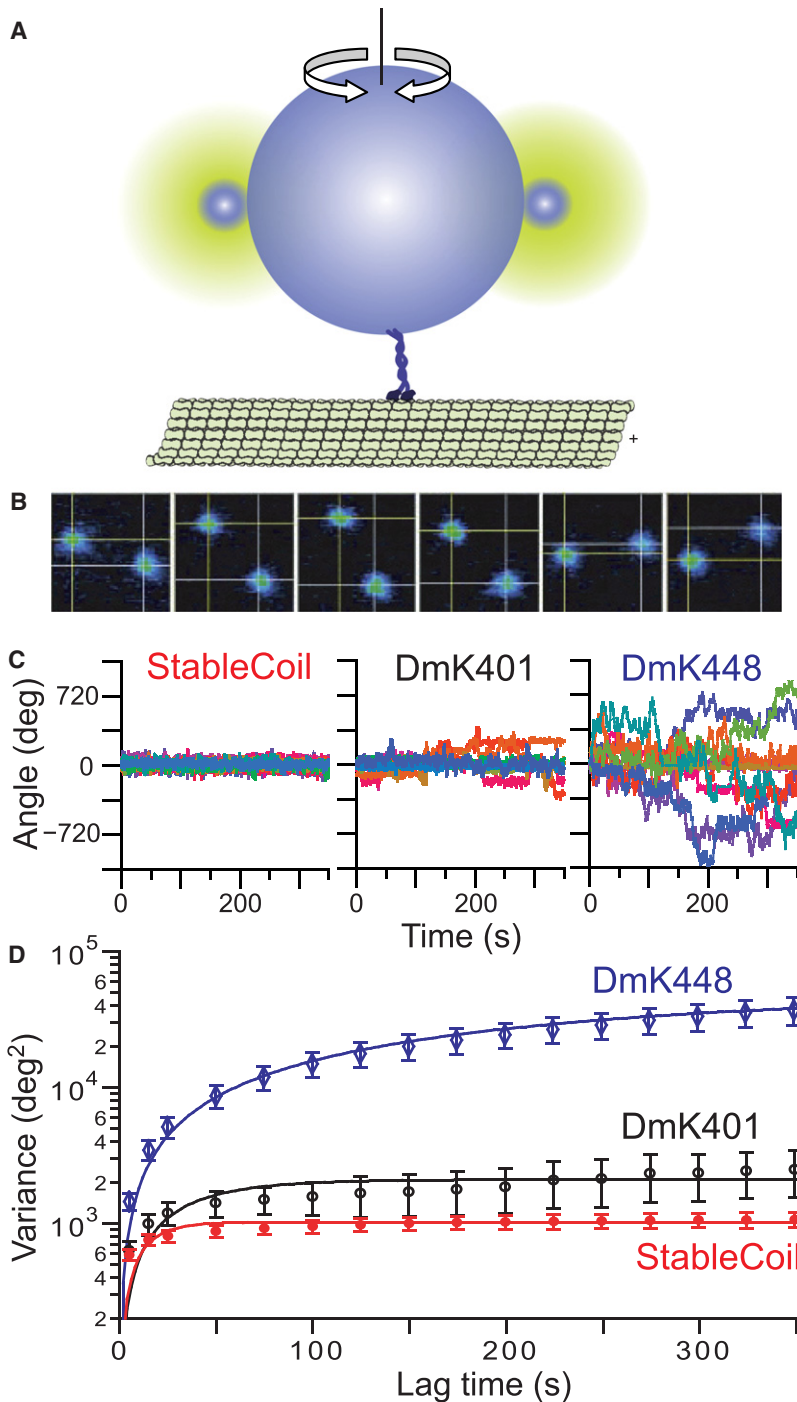
FIGURE 3 Measurements of torsional stiffness. (*A*) Cartoon illustrating the experimental geometry (not to scale), with a bead-bound kinesin molecule (*dark gray, blue* online) attached to a MT. The large central bead has two small fluorescent marker beads (*faint halos*) bound on opposite sides. (*B*) Sequence of video images showing marker bead positions (*pseudocolor* online) overlaid by cursors from centroid tracking, from which the azimuthal angle is computed ($\Delta t = 1$ s; field of view ~2 μm × 2 μm). (*C*) Single-molecule records of angle versus time showing rotation of three different kinesin constructs. (*D*) Average variance against lag time for the data in *C*, DmK448 (*open diamonds*; $N = 10$), DmK401 (*open circles*; $N = 14$) and StableCoil (*solid circles*; $N = 17$), with standard errors. Line fits are to exponentials used to extract the asymptotic variance, which supplies the torsional stiffness (see Materials and Methods).

of −4.1 pN. Evidently, the stiffness can vary over 50-fold without significantly affecting the limp factor, a finding that argues strongly against winding models.

Due to the experimental geometry, the hindering or assisting loads applied by an optical trap to bead-borne kinesin molecules moving along a MT necessarily include a vertical component, F_z, as well as a longitudinal component in the specimen plane, F_x. The balance of these components is related to the angle between the MT long axis and the kinesin stalk, θ, according to $F_z = F_x \tan \theta$ (Fig. 4 *A*). We probed the effect of vertical loading on limping in two ways: changing the angle under constant longitudinal load, and changing the value of the longitudinal load at (approximately) fixed angle. For the first test, we attached DmK612 molecules, which have comparatively long stalks, to beads of various sizes, calculated to produce changes in angle from 49° to 63°. Increasing the angle caused limping to increase dramatically, from $L = 2.2$ to 7.5 (Fig. 4 *B*). Data from previous assays with constant bead size, but different stalk length (which also change the angle), display the same trend (1).
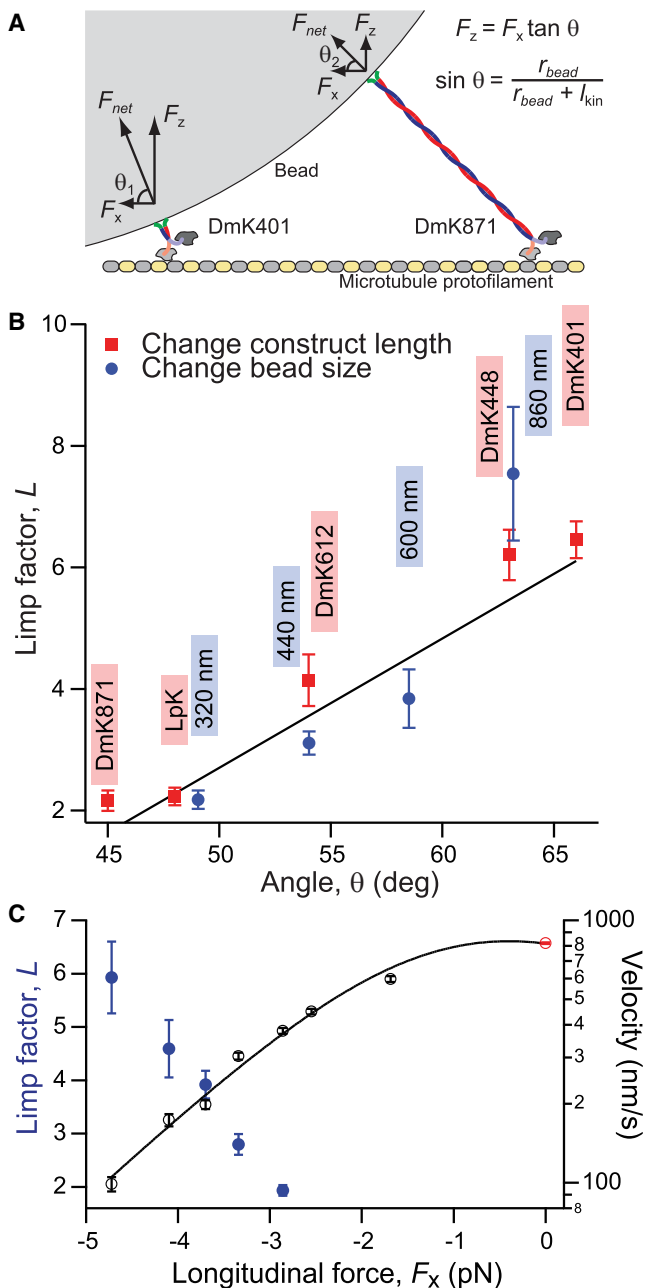
FIGURE 4 Modulating the vertical force by changing the angle or value of the applied load. (*A*) Cartoon illustrating the geometric relationship between force and angle of applied load for two constructs of different stalk lengths bound to the same bead. In a force clamp, the same longitudinal force, F_x, is experienced by both, but due to differences in angle, the vertical components and total force on the motors differ. (*B*) Limp factors for DmK612 motors attached to beads of various diameters (*solid circles*; $F_x = -4.0$ pN) and for constructs of various lengths attached to 0.44 μm diameter beads (*solid squares*; $F_x \sim -5$ pN; data from Asbury et al. (1)) are plotted against angle. LpK is native squid kinesin (data from Asbury et al. (1)). The line is a linear fit to all data. (*C*) Mean limp factor (*solid circles*) and velocity (*black and light gray, red* online; with curve fit) against longitudinal load for DmK401 motors attached to 0.44 μm diameter beads. The light gray (*red* online) open circle indicates the unloaded velocity, measured by video tracking. Each point represents data from at least 80 stepping records from 10 molecules. All assays were carried out at 2 mM ATP.

For the second test of vertical load, we kept the angle nearly constant, using DmK401 motors attached to 440-nm diameter beads, and varied the longitudinal load. Previous work had suggested that the degree of limping increased under large longitudinal (hindering) loads (11); however, those experiments were not carried out under force-clamped conditions. We therefore revisited this experiment to facilitate comparisons with our data sets. High hindering loads on kinesin molecules reduced the average stepping velocity in a Boltzmann-type manner, as previously found for non-limping kinesin motors (Figs. 1 *B* and 4 *C*) (19). Changing the longitudinal and vertical loads simultaneously strongly affected limping, consistent with Higuchi et al. (11): as the longitudinal load increased from -2.8 to -4.7 pN, L increased from ~2 to ~6 (Fig. 4 *C*). The simplest interpretation of these data, given the correlation between L and stalk angle found earlier, is that high external loads increase L by increasing the vertical component of the load.

Models of kinesin mechanochemistry that incorporate sensitivity to vertical loads require that some portion of the molecule execute motions in a vertical direction during the reaction cycle. The neck linkers and the neck coiled-coil domain have been proposed to undertake such motions (12,18), making these regions an attractive target for mutation and chemical manipulation. We engineered an additional mutant to introduce a reversible cross-link closer to the neck linkers, hypothesizing that this construct might exhibit chemical control of limping, depending on the presence or absence of the disulfide bond. Y352C is located one α-helical repeat from the start of the neck coiled coil, and one repeat closer to the heads than N359C. Just as with N359C, Y352C exhibited severe limping under reducing conditions ($L = 5.1 \pm 0.6$; no cross-link; $F_x = -4.1$ pN.). However, under oxidizing conditions, Y352C molecules exhibited a reduction in limping ($L = 2.8 \pm 0.2$; cross-linked) compared to DmK401 ($L = 4.9 \pm 0.4$)(Fig. S1 in the Supporting Material). Furthermore, the average velocity of Y352C mutants in oxidizing buffer was faster than under reducing conditions: $v = 232 \pm 9$ nm/s (oxidizing; $N = 122$) versus $v = 182 \pm 12$ nm/s (reducing; $N = 68$). Taken all together, these observations focus attention on the neck coiled-coil region as a locus for limping; possible mechanisms are discussed below.

DISCUSSION

The finding that recombinant kinesin constructs with long stalks tend to limp less than those with short ones (1) suggests that some property of the stalk domain may play a role in breaking the symmetry of stepping. Among the possibilities considered here were some kind of misregistration of the coiled coil in the neck region (which would lead to asymmetry in the lengths of the neck linkers), over- or under-winding of the coiled coil during stepping (which would lead to asymmetry in the torsion exerted by the stalk), and vertical loading of the molecule (which would lead to asymmetry in force for
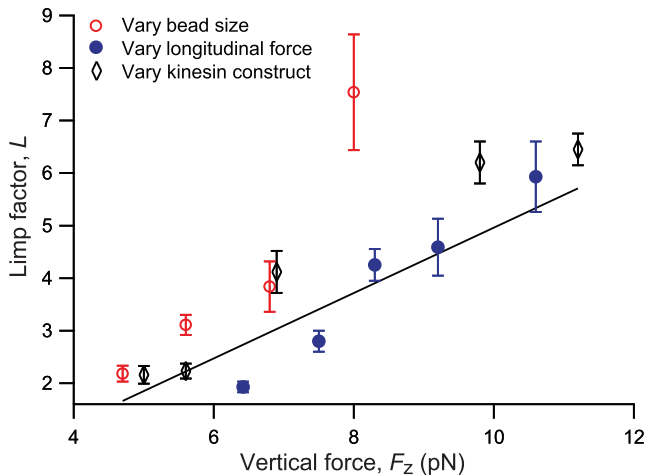
FIGURE 5 Limping versus vertical load. The three data sets in Fig. 4 are replotted against the computed vertical load, DmK612 motors bound to various-sized beads under fixed longitudinal load (*open circles*); DmK401 motors bound to 0.44 μm diameter beads under varying longitudinal loads (*solid circles*) and kinesin constructs of various stalk lengths bound to 0.44 μm diameter beads under fixed longitudinal load (*open diamonds*, data from Asbury et al. (1)). The line is a linear fit to all data.

certain types of structure). We tested for possible misregistration by engineering the N359C mutant, which will only form an intramolecular cross-link when its α-helices are in perfect register. The finding that this construct cross-links with high efficiency and continues to limp while cross-linked rules out misregistration as a candidate mechanism. To test the winding model, we developed an assay to measure the rotational properties of kinesin molecules bound to MTs, examining three constructs of different stalk composition, which collectively exhibited a ~50-fold range in torsional stiffness. Despite this large variation in stiffness, the mutants displayed similar degrees of limping. Therefore, a mechanism where limping is caused by differential torsional stiffness, such as over- and underwinding, is likely excluded.

In a single-molecule bead assay, the vector of force applied by an optical trap to the kinesin motor is necessarily angled upward with respect to the MT, due to the finite size of the bead, causing the molecule to be loaded both longitudinally and vertically. We compared data from three experiments to identify which parameter—the angle of the applied load, the longitudinal load, or the vertical load—was most influential in determining the limp factor. The only parameter to consistently correlate with the limp factor was the magnitude of the vertical load, and the data can be replotted to illustrate this correlation (Fig. 5). Taken all together, our data support a mechanism for kinesin limping that is sensitive to the vertical component of the load.

It has been reported that vertical loads affect the velocity of kinesin-driven movement. The Howard group analyzed the buckling behavior of a MT clamped at one end to a cover glass surface but propelled at its opposite end by a single kinesin molecule, a geometry that applies both vertical and (hindering) longitudinal loads to the motor. Surprisingly, kinesin molecules in that assay moved faster under increased vertical loads (17). By contrast, Fisher and Kim proposed an energy landscape model for kinesin motion where the molecule rises and falls relative to the MT during the course of every step, and which predicts that vertical loads would slow stepping (18). The observation that limping depends upon vertical load suggests a differential force sensitivity for each head during hand-over-hand motion. In terms of an energy landscape, limping implies that the transition state for stepping lies at a different height for alternate steps. We found previously that increases in limping tend to selectively lengthen the dwell intervals of the slower step phase, but leave the timing of the faster step phase mostly unchanged (1). The slower kinetics of the affected head for $F_z > 0$ may be consistent with the stepping mechanism proposed by Fisher and Kim (18), but only for alternate steps.

We did not discover any set of conditions under which vertical loads would speed up the timing of kinesin stepping, as reported by Gittes et al. (17). However, MT buckling experiments provide only an indirect readout of the force, based on modeling the MT elasticity and fits to theoretical curves, and the results can be sensitive to errors in digitizing the shapes of MTs. It is also possible that these experiments supplied combinations of forces not attained in our assays.

In an asymmetric hand-over-hand walk, alternate steps have different trajectories, despite being executed by heads with identical polypeptide composition. This property has been incorporated into notional sequences of hand-over-hand motion, which often show the trailing head swinging up and over the leading head for one step (i.e., moving in a vertical plane), but the newly trailing head swinging around to the side of the newly leading head (i.e., moving in a horizontal plane) for the subsequent step (28,29). Note that the two trajectories differ in the extent of vertical motion during a step. To explain limping in kinesin homodimers (1,11), Xie and co-workers proposed a kinetic model where structural differences in stalk orientation lead to "different vertical forces acting on the kinesin head in two successive steps" (12). Their mechanistic model combines known features of kinesin biochemistry with vectorial aspects of the loading geometry, and accounts for the existing data. The data in Figs. 4 C and 5 confirm a prediction that the limp factor would increase with greater longitudinal and vertical loading.

What portion of the kinesin molecule is chiefly responsible for its sensitivity to vertical load? The most likely candidates to execute up-and-down motion and also to affect stepping kinetics are the neck linkers themselves and the region where they coalesce to form the stalk, in the N-terminal domain of the neck (12,18). Results from the mutant Y352C directly implicate the neck coiled coil as a determinant of limping, because the severity of limping could be reversibly modulated by forming a cross-link in this region. The average velocity of cross-linked Y352C constructs was faster than for non-cross-linked constructs, suggesting that cross-linking accelerates

an otherwise slow transition rate, rather than causing some new biochemical transition to become rate-limiting. The neck coiled coil has attributes that position it uniquely to affect stepping kinetics. During processive stepping, it is thought that the reaction cycles of the kinesin heads are maintained out of phase (''gated'') by mechanical strain transmitted via the neck linkers through the neck coiled coil (24). A key structural element of this transmission would be the α-helix capping motif, spanning residues 343–349 (in *Drosophila melanogaster*), which stabilizes the N-terminus of coiled coil (30). It seems possible that differential up-and-down movements during alternating steps are accommodated by structural asymmetries in these capping motifs, which are disrupted by a cross-link at nearby position 352.

In summary, we find that kinesin homodimer constructs limp not because they become misregistered in their coiled coils, nor because they are torsionally asymmetric, but because certain structural elements located near the heads are differentially sensitive to vertical loading. Kinesin moves by an asymmetric hand-over-hand walk, and therefore the trajectories of its two heads are intrinsically different during alternate steps. The sensitivity of limping to vertical load implies that these trajectories must involve different amounts of vertical motion. Finally, the ability to reversibly control limping with a disulfide bond between α-helices adjacent to the N-terminal cap of the coiled coil implicates this region as a determinant of limping. It therefore seems possible that the final heptad repeat of the neck coiled coil may ''breathe'' (reversibly associate and dissociate) and change structure dynamically during stepping. Future biostructural and nanomechanical work, concentrating on the neck coiled coil, should be able to provide additional insights into the mechanisms of gating and limping in kinesin.

SUPPORTING MATERIAL

REFERENCES

1. Asbury, C. L., A. N. Fehr, and S. M. Block. 2003. Kinesin moves by an asymmetric hand-over-hand mechanism. *Science*. 302:2130–2134.

2. Kaseda, K., H. Higuchi, and K. Hirose. 2003. Alternate fast and slow stepping of a heterodimeric kinesin molecule. *Nat. Cell Biol.* 5:1079–1082.

3. Yildiz, A., M. Tomishige, R. D. Vale, and P. R. Selvin. 2004. Kinesin walks hand-over-hand. *Science*. 303:676–678.

4. Coy, D. L., M. Wagenbach, and J. Howard. 1999. Kinesin takes one 8-nm step for each ATP that it hydrolyzes. *J. Biol. Chem.* 274:3667–3671.

5. Hua, W., E. C. Young, M. L. Fleming, and J. Gelles. 1997. Coupling of kinesin steps to ATP hydrolysis. *Nature*. 388:390–393.

6. Schnitzer, M. J., and S. M. Block. 1997. Kinesin hydrolyses one ATP per 8-nm step. *Nature*. 388:386–390.

7. Asbury, C. L. 2005. Kinesin: world's tiniest biped. *Curr. Opin. Cell Biol.* 17:89–97.

8. Block, S. M., L. S. Goldstein, and B. J. Schnapp. 1990. Bead movement by single kinesin molecules studied with optical tweezers. *Nature*. 348:348–352.

9. Svoboda, K., C. F. Schmidt, B. J. Schnapp, and S. M. Block. 1993. Direct observation of kinesin stepping by optical trapping interferometry. *Nature*. 365:721–727.

10. Vale, R. D., T. S. Reese, and M. P. Sheetz. 1985. Identification of a novel force-generating protein, kinesin, involved in microtubule-based motility. *Cell*. 42:39–50.

11. Higuchi, H., C. E. Bronner, H. W. Park, and S. A. Endow. 2004. Rapid double 8-nm steps by a kinesin mutant. *EMBO J.* 23:2993–2999.

12. Xie, P., S. X. Dou, and P. Y. Wang. 2007. Limping of homodimeric kinesin motors. *J. Mol. Biol.* 366:976–985.

13. Tomishige, M., and R. D. Vale. 2000. Controlling kinesin by reversible disulfide cross-linking: identifying the motility-producing conformational change. *J. Cell Biol.* 151:1081–1092.

14. Shao, Q., and Y. Q. Gao. 2007. Asymmetry in kinesin walking. *Biochemistry*. 46:9098–9106.

15. Bryant, Z., M. D. Stone, J. Gore, S. B. Smith, N. R. Cozzarelli, et al. 2003. Structural transitions and elasticity from torque measurements on DNA. *Nature*. 424:338–341.

16. Howard, J. 1996. The movement of kinesin along microtubules. *Annu. Rev. Physiol.* 58:703–729.

17. Gittes, F., E. Meyhofer, S. Baek, and J. Howard. 1996. Directional loading of the kinesin motor molecule as it buckles a microtubule. *Biophys. J.* 70:418–429.

18. Fisher, M. E., and Y. C. Kim. 2005. Kinesin crouches to sprint but resists pushing. *Proc. Natl. Acad. Sci. USA*. 102:16209–16214.

19. Block, S. M., C. L. Asbury, J. W. Shaevitz, and M. J. Lang. 2003. Probing the kinesin reaction cycle with a 2D optical force clamp. *Proc. Natl. Acad. Sci. USA*. 100:2351–2356.

20. Lang, M. J., C. L. Asbury, J. W. Shaevitz, and S. M. Block. 2002. An automated two-dimensional optical force clamp for single molecule studies. *Biophys. J.* 83:491–501.

21. Lupas, A., M. Van Dyke, and J. Stock. 1991. Predicting coiled coils from protein sequences. *Science*. 252:1162–1164.

22. Visscher, K., M. J. Schnitzer, and S. M. Block. 1999. Single kinesin molecules studied with a molecular force clamp. *Nature*. 400:184–189.

23. Valentine, M. T., P. M. Fordyce, T. C. Krzysiak, S. P. Gilbert, and S. M. Block. 2006. Individual dimers of the mitotic kinesin motor Eg5 step processively and support substantial loads in vitro. *Nat. Cell Biol.* 8:470–476.

24. Guydosh, N. R., and S. M. Block. 2006. Backsteps induced by nucleotide analogs suggest the front head of kinesin is gated by strain. *Proc. Natl. Acad. Sci. USA*. 103:8054–8059.

25. Neuman, K. C., and S. M. Block. 2004. Optical trapping. *Rev. Sci. Instrum.* 75:2787–2809.

26. Fehr, A. N., C. L. Asbury, and S. M. Block. 2008. Kinesin steps do not alternate in size. *Biophys. J.* 94:L20–L22.

27. Stryer, L. 1995. Biochemistry. W.H. Freeman and Company, New York.

28. Hoenger, A., M. Thormahlen, R. Diaz-Avalos, M. Doerhoefer, K. N. Goldie, et al. 2000. A new look at the microtubule binding patterns of dimeric kinesins. *J. Mol. Biol.* 297:1087–1103.

29. Vale, R. D., and R. A. Milligan. 2000. The way things move: looking under the hood of molecular motor proteins. *Science*. 288:88–95.

30. Tripet, B., and R. S. Hodges. 2002. Helix capping interactions stabilize the N-terminus of the kinesin neck coiled-coil. *J. Struct. Biol.* 137:220–235.

On the origin of kinesin limping

Steven M. Block, Adrian N Fehr, Braulio Gutierrez-Medina, and Charles L Asbury

SUPPORTING MATERIAL for:

On the origin of kinesin limping

Adrian N. Fehr,* Braulio Gutiérrez-Medina,[†] Charles L. Asbury,[‡] and Steven M. Block*[†]

Departments of *Applied Physics and [†]Biology, Stanford University, Stanford, California 94305, and [‡]Department of Physiology & Biophysics, University of Washington, Seattle, Washington 98195
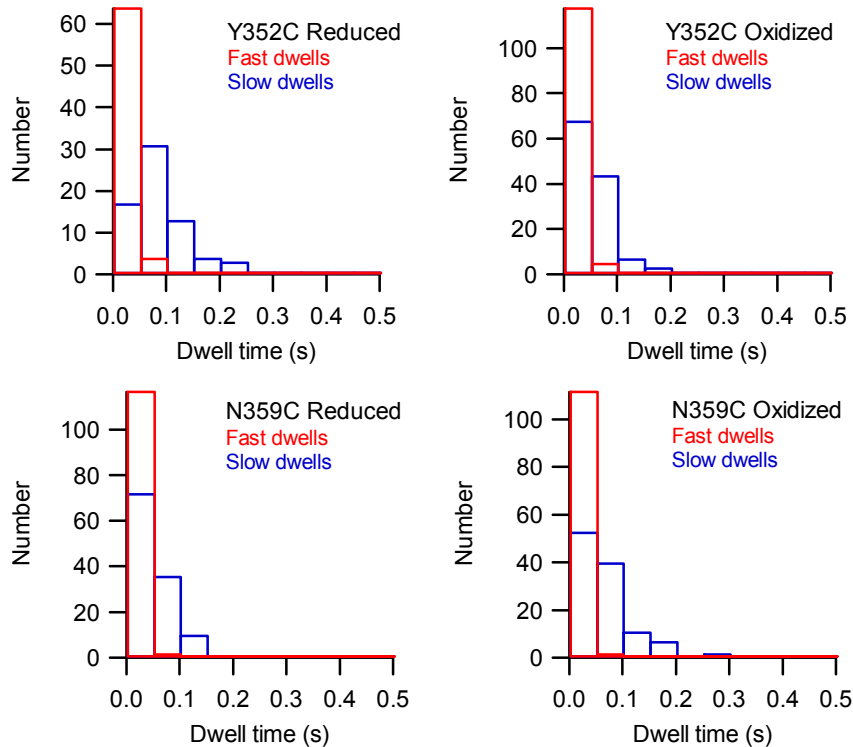
Supporting Figure S1. Histograms of the dwell-time distributions for the Y352C and N359C constructs under reduced or oxidizing conditions. Alternate (i.e., even- or odd-numbered) dwell intervals for individual runs were scored and separated into two sets, corresponding to 'fast' and 'slow' phases, based on the average time spent in each phase, as described in the main text and ref. 1 (Asbury *et al*., 2003, *Science* **302**: 2130-2134). Times for fast dwells (red) and slow dwells (blue) were compiled into histograms using a bin width of 0.05 s. The ratio of the average dwell time in the slow phase to the average dwell time in the fast phase supplies the limp factor for each run. The mean limp factor, L, was computed as an average of limp factors for all individual runs under a given set of conditions. **Upper panels**: *Left*, Y352C under reducing conditions (no cross-link), $L = 5.1 \pm 0.6$ (mean ± std. err.), based on $N = 68$ runs. *Right*, Y352C under oxidizing conditions (cross-linked), $L = 2.8 \pm 0.2$ (mean ± std. err.), based on $N = 122$ runs. **Lower panels**: *Left*, N359C under reducing conditions (no cross-link), $L = 3.7 \pm 0.3$ (mean ± std. err.), based on $N = 119$ runs. *Right*, N359C under oxidizing conditions (cross-linked), $L = 3.9 \pm 0.3$ (mean ± std. err.), based on $N = 114$ runs.